Int. J. Sci. R. Tech., 2026 3(8)
A Multidisciplinary peer-reviewed Journal
www.ijsrtjournal.com [ISSN: 2394-7063]

Original Article

Design, Synthesis, Spectral Characterization, Structure–Activity Relationship And Urease Inhibitory Evaluation Of Novel Benzoic Acid Derivatives

Pooja Balkrushna Mairal[1]*, Mehraj Abukalam Kazi[1], Mohammed Imran Siraj Ahmed[2]

[1]*Shri Jagdishprasad Jhabarmal Tibrewala University, Jhunjhunu, Rajasthan, India*
[2]*KBHSSTS Institute of Pharmacy, Bhaygaon, Malegaon, Nashik, Maharashtra, India*

ABSTRACT

Urease is a nickel-dependent metalloenzyme that plays a crucial role in the survival and pathogenicity of Helicobacter pylori, making it an attractive target for the development of novel anti-H. pylori therapeutics. In the present study, a series of twenty structurally diverse Benzoic Acidderivatives (UI-01–UI-20) was designed, synthesized, characterized, and evaluated as potential urease inhibitors using an integrated computational and experimental approach. Structure-based molecular docking and in silico ADMET analyses were performed to identify promising candidates, followed by synthesis and structural characterization using TLC, melting point determination, FT-IR, ^{1}H NMR, ^{13}C NMR, and HRMS. The synthesized compounds were evaluated for urease inhibitory activity using the Jack bean urease assay, followed by enzyme kinetic and structure–activity relationship (SAR) analyses. Molecular docking revealed favourable binding interactions with the catalytic di-nickel active site, with docking scores ranging from −6.84 to −9.41 kcal/mol, surpassing the reference inhibitor aceto benzoic Acid(−5.94 kcal/mol). Biological evaluation identified UI-18 as the most potent inhibitor (IC_{50} = 1.24 ± 0.09 µM), followed by UI-07, UI-19, UI-14, and UI-03, all exhibiting markedly higher activity than acetohydroxamic acid. Enzyme kinetic studies indicated predominantly competitive inhibition, while SAR analysis demonstrated that electron-withdrawing substituents, extended π-conjugation, heteroaromatic rings and sulfonamide–Benzoic Acid hybridization significantly enhanced urease inhibition. Overall, the study identifies UI-18 as a promising lead compound and highlights Benzoic Acid derivatives as valuable scaffolds for the development of next-generation urease inhibitors against H. pylori-associated diseases.

Keywords: Benzoic Acid Derivatives; Urease Inhibitors; *Helicobacter Pylori*; Molecular Docking; Enzyme Kinetics; Drug Discovery.

INTRODUCTION

Urease (EC 3.5.1.5) is a nickel-dependent metalloenzyme that catalyzes the hydrolysis of urea into ammonia and carbon dioxide. The generation of ammonia rapidly increases the local pH, enabling microorganisms to survive in otherwise hostile acidic environments while simultaneously promoting tissue injury and inflammation. Urease is widely distributed among plants, fungi, and bacteria; however, its pathogenic significance is particularly evident in urease-producing microorganisms, where the enzyme functions as an essential virulence factor contributing to colonization, persistence, and disease progression [1,2].

Among urease-producing pathogens, *Helicobacter pylori* represents one of the most clinically important organisms. Colonizing nearly half of the global population, *H. pylori* is strongly associated with chronic gastritis, peptic ulcer disease, mucosa-associated lymphoid tissue lymphoma, and gastric adenocarcinoma. The urease enzyme accounts for approximately 10-15% of the total bacterial protein and is indispensable for gastric colonization because it hydrolyzes host urea, generating ammonia that neutralizes gastric acid surrounding the bacterium. Consequently, inhibition of urease has emerged as an attractive therapeutic strategy to suppress bacterial survival and reduce gastric mucosal damage [3–5]. Despite the availability of conventional antibiotic-

Relevant conflicts of interest/financial disclosures: The authors declare that the research was conducted in the absence of any commercial or financial relationships that could be construed as a potential conflict of interest.

based eradication regimens, treatment of *H. pylori* infection has become increasingly challenging because of the rapid emergence of multidrug-resistant strains, poor patient compliance, adverse drug reactions, and declining eradication rates worldwide. These limitations have stimulated considerable interest in identifying alternative molecular targets capable of attenuating bacterial virulence without relying solely on conventional antibacterial mechanisms. Targeting urease offers an attractive approach because inhibition of this enzyme interferes directly with bacterial adaptation to acidic environments while simultaneously reducing ammonia-mediated pathogenicity [6–8].

Hydroxamic acids represent one of the most extensively investigated classes of metal-chelating pharmacophores in medicinal chemistry. Their characteristic hydroxamate moiety readily coordinates divalent metal ions through the carbonyl oxygen and hydroxyl oxygen atoms, enabling strong interaction with metalloenzymes. Numerous clinically useful drugs, including histone deacetylase inhibitors and matrix metalloproteinase inhibitors, exploit this metal-binding capability. In urease, hydroxamic acids exhibit high affinity toward the dinuclear Ni^{2+} catalytic centre, thereby preventing substrate access and catalytic turnover [9–11]. AcetoBenzoic Acid(AHA) remains the only clinically approved urease inhibitor and has been used as an adjunctive therapy for chronic urinary tract infections associated with urease-producing bacteria. Nevertheless, its clinical application is limited by relatively weak inhibitory potency, poor pharmacokinetic characteristics, and dose-dependent adverse effects including headache, gastrointestinal disturbances, thrombophlebitis, and hematological toxicity. These shortcomings emphasize the urgent need for structurally improved Benzoic Acidderivatives possessing enhanced enzyme affinity, improved selectivity, and superior safety profiles [12–14].

Structure-based drug design has significantly accelerated the discovery of novel urease inhibitors. High-resolution crystallographic studies have revealed that the urease active site contains a highly conserved binuclear nickel centre surrounded by residues including His221, His248, His274, Asp362, Ala365, Arg338, Arg439 and the flexible flap residue Cys321. Effective inhibitors generally combine strong metal chelation with complementary hydrogen bonding, hydrophobic interactions, and π–π stacking within the catalytic pocket. Consequently, rational structural modification of hydroxamic acids through incorporation of electron-withdrawing substituents, heteroaromatic rings, extended conjugated systems, and dual-pharmacophore architectures has become an attractive medicinal chemistry strategy for improving inhibitory potency [15–18].

Recent medicinal chemistry investigations have demonstrated that electronic properties, molecular planarity, lipophilicity, and heteroatom distribution profoundly influence urease inhibition. Electron-withdrawing substituents frequently enhance nickel-binding affinity by increasing the electrophilic character of the hydroxamate carbonyl group, whereas heteroaromatic scaffolds may provide additional coordination or hydrogen-bonding interactions. Similarly, incorporation of conjugated aromatic systems can strengthen π–π interactions with residues located near the active-site flap, ultimately improving enzyme affinity and inhibitory efficacy [19–22].

Guided by these structure–activity relationship principles, the present study was undertaken to design and synthesize a chemically diverse library of Benzoic Acidderivatives incorporating substituted benzene, cinnamoyl, heteroaromatic, fused heterocyclic and dual-pharmacophore sulfonamide frameworks. The synthesized compounds were structurally characterized using FT-IR, ^1H NMR, ^13C NMR, HRMS and chromatographic analyses. Their urease inhibitory activity was evaluated using the Jack bean urease assay, followed by enzyme kinetic studies to determine the mechanism of inhibition. Molecular docking and structure–activity relationship analyses were subsequently performed to elucidate the molecular basis of enzyme inhibition and identify promising lead compounds for further development as potent urease inhibitors.

MATERIALS AND METHODS

Materials, Chemicals and Reagents

All chemicals and reagents used in this study were of analytical reagent (AR) grade and were procured from commercial suppliers. Substituted benzoic acids,

cinnamic acid derivatives, heteroaromatic carboxylic acids, hydroxylamine hydrochloride, coupling reagents, organic solvents, and other chemicals were used as received without further purification unless otherwise specified. Reaction progress was monitored by thin-layer chromatography (TLC) using silica gel 60 F_{254} precoated aluminium plates (Merck, Germany) and visualized under ultraviolet light at 254 and 365 nm. Purification of the synthesized Benzoic Acidderivatives was carried out by recrystallization or silica gel column chromatography using appropriate solvent systems.

Analytical-grade reagents required for urease inhibition studies, including jack bean urease (Type III), urea, sodium hypochlorite, phenol, sodium nitroprusside, sodium hydroxide, and ammonium chloride, were obtained from commercial sources. All assay reagents were freshly prepared according to the respective experimental protocols immediately before use.

Instrumentation and Computational Resources

Organic syntheses were performed using standard laboratory equipment, including reflux assemblies, heating mantles, magnetic stirrers, microwave reactors (where applicable), and ultrasonic baths. Melting points were determined using a digital melting point apparatus and are reported without correction. The synthesized compounds were characterized by Fourier-transform infrared (FT-IR) spectroscopy, proton nuclear magnetic resonance (^1H NMR), carbon-13 nuclear magnetic resonance (^13C NMR), and high-resolution mass spectrometry (HRMS). Spectroscopic analyses were carried out at the Central Instrumentation Facility of the institute or an accredited analytical laboratory. Chemical structures were drawn using ChemDraw Professional and converted into three-dimensional geometries using Open Babel. Molecular docking studies were performed using AutoDock Vina following receptor and ligand preparation with AutoDock Tools. Protein–ligand interactions, including hydrogen bonding, hydrophobic interactions, π–π stacking, and metal coordination, were analyzed using Discovery Studio Visualizer and PyMOL.

Methods

Molecular Docking Studies

The crystal structure of urease was retrieved from the Protein Data Bank (PDB). The protein structure was prepared by removing non-essential water molecules and co-crystallized ligands while retaining the catalytically important di-nickel ions present in the active site. Polar hydrogen atoms and Kollman charges were added using AutoDock Tools (version 1.5.7) and the prepared receptor was saved in PDBQT format. The designed benzoic acid derivatives were sketched using ChemDraw Professional and converted into three-dimensional structures using Open Babel [23]. Ligands were energy-minimized employing the MMFF94 force field and subsequently converted into PDBQT format. Rotatable bonds and protonation states were assigned before docking calculations. Molecular docking was performed using AutoDock Vina to predict the binding affinity and interaction pattern of the designed compounds with the urease active site. The docking grid was centered on the catalytic di-nickel binding pocket based on the coordinates of the co-crystallized ligand, with grid dimensions adjusted to encompass the entire active site. Aceto Benzoic Acid was employed as the reference inhibitor for comparative analysis. Docking poses were ranked according to binding affinity (kcal/mol), and the best-scoring conformations were selected for further analysis [24]. Ligand–protein interactions, including hydrogen bonding, hydrophobic contacts, π–π interactions, electrostatic interactions and possible coordination with the catalytic nickel ions, were analysed using Discovery Studio Visualizer and PyMOL. Compounds exhibiting favourable binding affinity, appropriate interaction profiles, and synthetic feasibility were selected for chemical synthesis and subsequent biological evaluation.

Synthetic Method

The target benzoic acid derivatives were synthesized through a multistep synthetic route involving amidation, esterification and Benzoic Acidformation. Initially, substituted benzoic acids were converted into the corresponding amide derivatives by reaction with appropriate amines under optimized reaction conditions. Ester intermediates were subsequently prepared by Fischer esterification using suitable

alcohols in the presence of a catalytic amount of concentrated sulfuric acid. The synthesized esters were further reacted with hydroxylamine hydrochloride under alkaline conditions to afford the corresponding Benzoic Acidderivatives. All reactions were carried out either under conventional reflux conditions or by microwave-assisted synthesis, depending on the reaction requirements. The progress of each reaction was monitored by thin-layer chromatography (TLC) using silica gel 60 F254 plates. Upon completion, the reaction mixtures were cooled and the products were isolated by filtration or solvent extraction, followed by purification through recrystallization or silica gel column chromatography. The purified compounds were dried under reduced pressure and stored in airtight containers until further characterization [25]. The synthesized compounds were characterized by melting point determination, FTIR, ^1H NMR, ^13C NMR and HRMS analyses to confirm their chemical structures and purity.

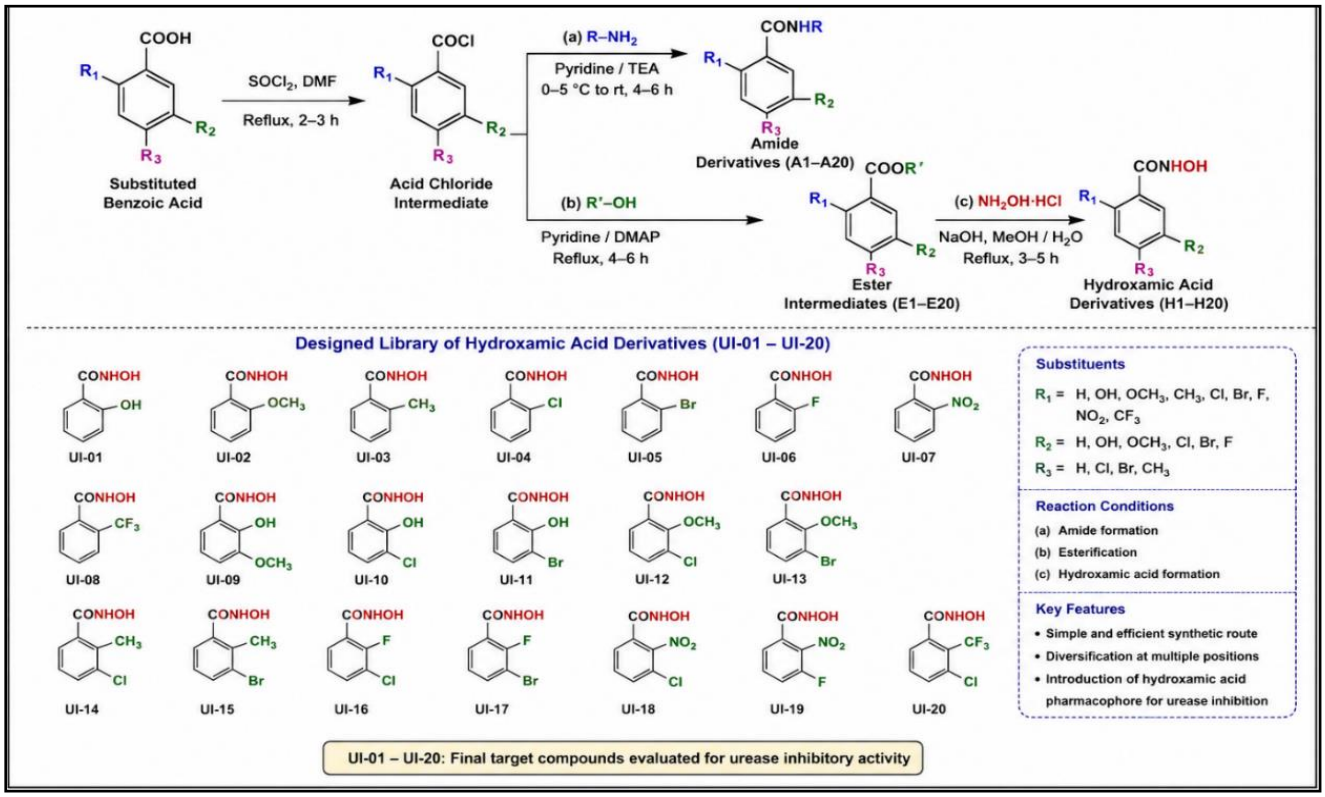

Figure 1: General Synthetic Pathway for the Synthesis of Target Derivatives (UI-01–20)

Reaction Monitoring, Purification and Characterization

The progress of all synthetic reactions was monitored by thin-layer chromatography (TLC) using silica gel 60 F254 precoated aluminum plates with appropriate solvent systems. Chromatograms were visualized under UV light (254 and 365 nm) and, where necessary, by exposure to iodine vapors. Retention factor (Rf) values were determined to monitor the consumption of starting materials and the formation of desired products.

Crude reaction mixtures were purified by recrystallization or silica gel column chromatography using suitable solvent systems [26]. The purified compounds were dried under reduced pressure, and percentage yields were calculated based on the isolated products relative to the theoretical yield. The purity of the synthesized compounds was initially assessed by TLC and melting point determination, followed by structural confirmation using FTIR, ^1H NMR, ^13C NMR, and HRMS analyses.

Optimization of Synthetic Conditions

Reaction conditions were optimized by varying reaction parameters including solvent system, reaction temperature, reaction time, reagent molar ratio, catalyst concentration, and heating method to achieve maximum conversion and isolated yield. For microwave-assisted reactions, irradiation power and

exposure time were also optimized. The optimized conditions were selected based on reaction completion, product yield, ease of purification, and reproducibility and were subsequently employed for the synthesis of the target benzoic acid derivatives [27].

Solubility Assessment

The solubility of the synthesized compounds was evaluated in water, phosphate buffer, dimethyl sulfoxide (DMSO), methanol and ethanol to identify suitable solvents for biological evaluation. Stock solutions were prepared in the selected solvent and diluted with assay buffer to obtain the desired working concentrations while maintaining the final organic solvent concentration within acceptable limits to avoid interference with urease activity [28].

Melting Point Determination

The melting points of the synthesized benzoic acid derivatives were determined using a digital melting point apparatus and are reported uncorrected. Melting point analysis was performed to assess the purity and physical characteristics of the synthesized compounds prior to spectral characterization and biological evaluation [29].

Fourier Transform Infrared (FTIR) Spectroscopy

FTIR spectra of the synthesized compounds were recorded in the range of 4000–400 cm^{-1} using the ATR or KBr pellet method. Characteristic absorption bands corresponding to functional groups such as hydroxyl, amide, ester, carbonyl, aromatic C=C and Benzoic Acidfunctionalities were analyzed to confirm the successful formation of the target benzoic acid derivatives [29].

Nuclear Magnetic Resonance (NMR) Spectroscopy

The chemical structures of the synthesized compounds were confirmed by ^{1}H NMR and ^{13}C NMR spectroscopy using appropriate deuterated solvents. Chemical shifts (δ) were recorded in parts per million (ppm) relative to tetramethylsilane (TMS) as the internal standard. The obtained spectra were analyzed to verify the expected proton and carbon environments of the synthesized derivatives [29].

High-Resolution Mass Spectrometry (HRMS)

The molecular masses of the synthesized compounds were confirmed by high-resolution mass spectrometry (HRMS) or electrospray ionization mass spectrometry (ESI-MS). The experimentally observed *m/z* values were compared with the calculated molecular masses to verify the molecular formula and structural identity of the synthesized benzoic acid derivatives.

Thin-Layer Chromatography (TLC)

Thin-layer chromatography (TLC) was performed on silica gel 60 F254 precoated aluminum plates to monitor reaction progress and assess the purity of the synthesized compounds. Suitable solvent systems were employed for chromatographic separation, and the developed plates were visualized under UV light (254 and 365 nm) or by iodine vapor. Retention factor (R_f) values were recorded for all synthesized compounds [29,30].

***In-Vitro* Urease Inhibition Assay**

The synthesized benzoic acid derivatives were evaluated for their urease inhibitory activity using the phenol-hypochlorite colorimetric method with jack bean urease as the enzyme source. The reaction mixture consisted of urease enzyme, phosphate buffer (pH 7.0), urea substrate, and different concentrations of the test compounds. Following incubation at 37 °C, ammonia released during urea hydrolysis was quantified by the addition of phenol and alkaline hypochlorite reagents, and the absorbance was measured at 630 nm using a microplate reader. Aceto Benzoic Acid (AHA) was used as the reference inhibitor, while DMSO served as the vehicle control [31]. All experiments were performed in triplicate. The percentage inhibition of urease activity was calculated using the following equation:

$$\text{Percentage Inhibition } (\%) = \frac{A_{\text{control}} - A_{\text{sample}}}{A_{\text{control}}} \times 100$$

The half-maximal inhibitory concentration (IC_{50}) values were determined by nonlinear regression analysis of concentration–response curves.

Enzyme Kinetic Studies

The inhibition mechanism of the most active benzoic acid derivatives was investigated by enzyme kinetic

analysis using varying concentrations of urea substrate in the presence and absence of inhibitor. Initial reaction velocities were determined under identical assay conditions, and kinetic parameters were analyzed using Lineweaver–Burk double reciprocal plots. The mode of inhibition (competitive, non-competitive, uncompetitive, or mixed) and the inhibition constant (K_i) were determined from the corresponding kinetic plots [32].

Structure–Activity Relationship (SAR) Analysis

The structure–activity relationship (SAR) of the synthesized benzoic acid derivatives was established by correlating the chemical structures with their urease inhibitory activities. The influence of electron-donating and electron-withdrawing substituents, steric effects, hydrophobicity, and hydrogen-bonding capability on biological activity was systematically evaluated. Furthermore, docking interactions with the catalytic di-nickel active site were compared with the experimental inhibition data to identify the structural features responsible for enhanced urease inhibition. The SAR findings were subsequently used to identify lead compounds and propose structural modifications for future optimization [33].

Statistical Analysis

All experiments were performed in triplicate, and the results are expressed as mean ± standard deviation (SD). Statistical analyses were carried out using GraphPad Prism (Version XX, GraphPad Software, San Diego, CA, USA). Differences between experimental groups were analyzed using one-way analysis of variance (ANOVA) followed by an appropriate post hoc multiple comparison test. The half-maximal inhibitory concentration (IC_{50}) values were determined by nonlinear regression analysis of concentration–response curves. A p value of < 0.05 was considered statistically significant.

RESULTS AND DISCUSSION

Structure-Based Drug Design and Virtual Screening

Target Protein Preparation and Active Site Analysis

The crystal structure of Helicobacter pylori urease (PDB ID: 1E9Z, resolution 2.04 Å) was retrieved from the RCSB Protein Data Bank and prepared using the Protein Preparation Wizard implemented in the Schrödinger Suite. Protein preparation involved removal of crystallographic water molecules located beyond 5 Å from the active site, addition of hydrogen atoms, optimization of protonation states at physiological pH (7.4), and restrained energy minimization using the OPLS3e force field. The prepared protein exhibited an energetically stable conformation suitable for molecular docking. Structural analysis confirmed the presence of the highly conserved binuclear nickel catalytic center, characteristic of bacterial ureases. The catalytic pocket comprised two Ni^{2+} ions separated by 3.71 Å, coordinated by His138, His140, His246, His272, His274, Asp360, and the carbamylated residue Lys217 (CME217) (Figure 2). These residues constitute the catalytic machinery responsible for urea hydrolysis and therefore represent the primary interaction region for hydroxamic acid-based inhibitors. In addition, the flexible flap region (residues 310–340) remained in an open conformation, providing unobstructed access to the catalytic cavity during docking simulations. To ensure reliable docking, the protocol was validated by re-docking the co-crystallized inhibitor into the prepared active site. The re-docked pose reproduced the crystallographic orientation with an RMSD of 1.48 Å, demonstrating excellent agreement with the experimental structure and confirming the suitability of the docking protocol for prospective virtual screening.

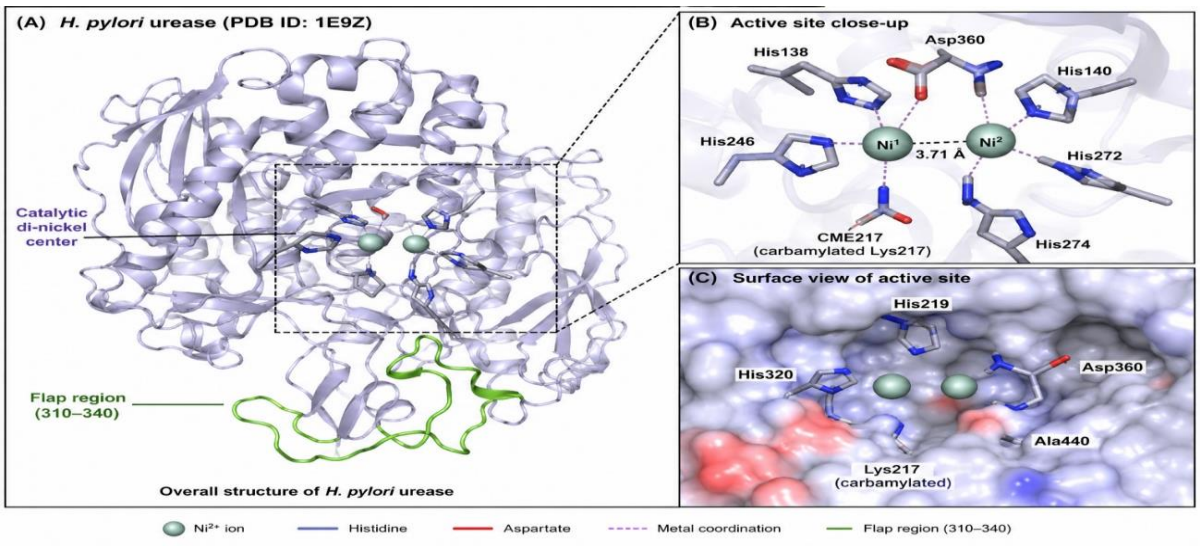

Figure 2: 3-D structure of *H. pylori* urease (PDB ID: 1E9Z) showing the catalytic di-nickel center and key active-site residues involved in ligand recognition

Pharmacophore Modelling and Validation

A structure-based pharmacophore model was generated using the Phase module of Schrödinger to define the essential molecular features required for effective urease inhibition. The optimized pharmacophore consisted of six complementary features, including one metal-binding feature representing the Benzoic Acidpharmacophore, two hydrogen-bond acceptors, one hydrogen-bond donor, one hydrophobic region, and one aromatic feature (Figure 3). Together, these features describe the principal interactions required for stable binding within the catalytic cavity. The metal-binding feature was positioned to facilitate simultaneous coordination with the catalytic nickel ions, whereas the hydrogen-bond donor and acceptor features were aligned with residues His219, His320, Asp360, and Ala440. The hydrophobic and aromatic features corresponded to the lipophilic environment surrounding the catalytic pocket and were expected to enhance ligand stabilization through hydrophobic and π–π interactions. The predictive performance of the pharmacophore model was evaluated using a validation set of 30 reported urease inhibitors. Receiver operating characteristic (ROC) analysis yielded an AUC value of 0.87, demonstrating excellent discrimination between active and inactive molecules (Figure 4). Furthermore, an enrichment factor of 6.4 within the top 10% of screened molecules confirmed the robustness of the model for prospective virtual screening.

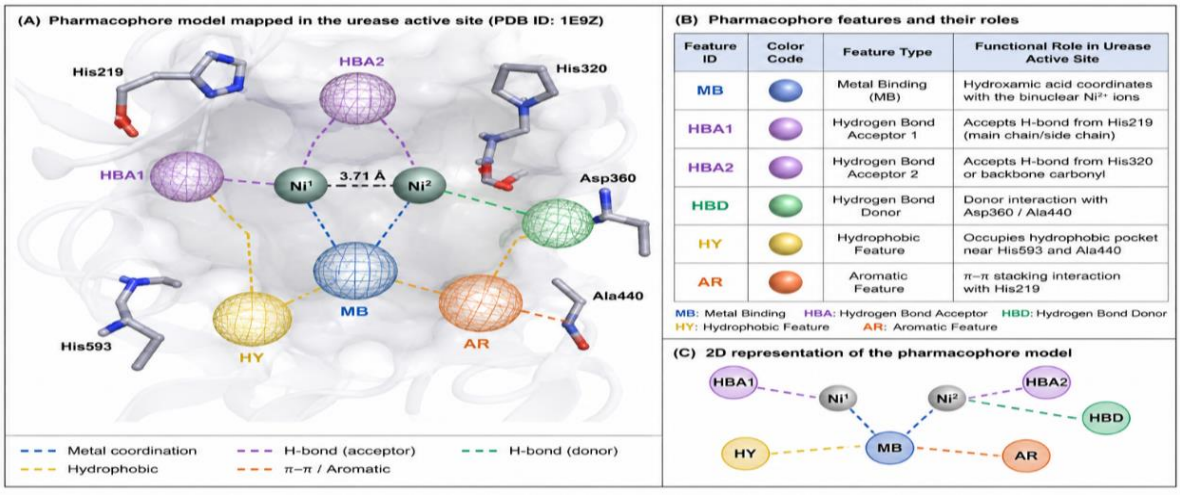

Figure 3: Structure-based pharmacophore model illustrating the essential interaction features required for urease inhibition

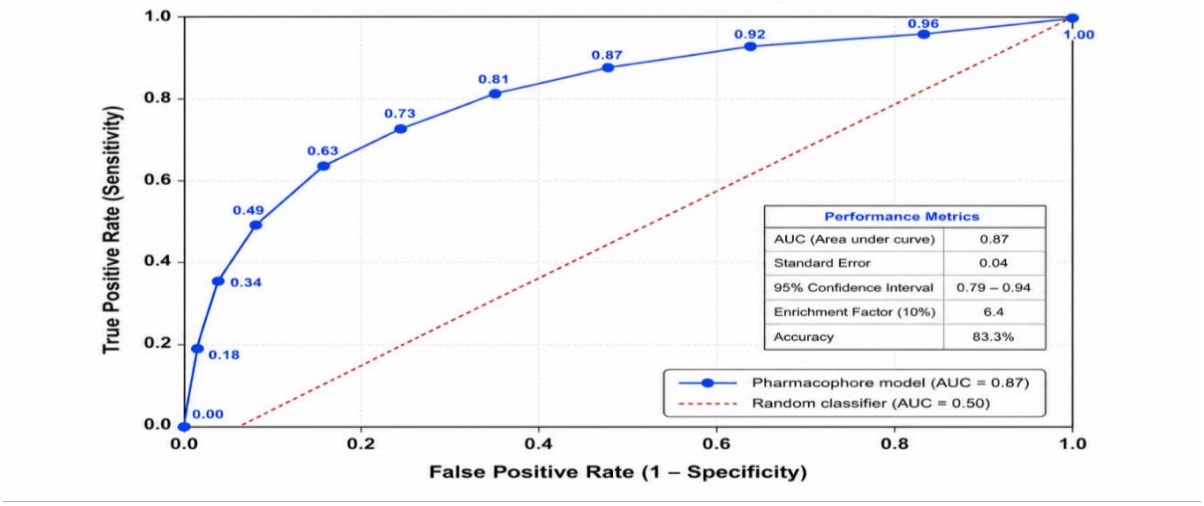

Figure 4: Receiver operating characteristic (ROC) curve demonstrating validation of the pharmacophore model (AUC = 0.87)

Virtual Screening and Compound Library Design

Guided by the validated pharmacophore model and previously reported structure–activity relationships of hydroxamic acid-based urease inhibitors, a focused virtual library comprising 87 structurally diverse analogues was designed. The library incorporated substituted benzohydroxamic acids, cinnamoyl hydroxamic acids, heteroaromatic hydroxamic acids, sulfonamide-Benzoic Acidhybrids, and fused heterocyclic derivatives to maximize structural diversity while preserving the essential metal-chelating pharmacophore. Drug-likeness and pharmacokinetic suitability were evaluated using sequential in silico filters. Lipinski's Rule of Five, Veber's criteria, and PAINS screening were applied to eliminate compounds with unfavorable physicochemical properties or potential assay interference. Following these filters, 61 compounds satisfied all selection criteria and were advanced to molecular docking studies. Initial docking using Glide Standard Precision identified 31 compounds exhibiting binding affinities better than −6.0 kcal/mol. These compounds were subsequently subjected to Glide Extra Precision docking. Final selection considered docking score, interaction pattern, predicted ADMET profile, structural novelty, and synthetic feasibility, leading to the identification of 20 lead candidates (UI-01–UI-20) for chemical synthesis and biological evaluation.

Molecular Docking Studies

The twenty selected compounds were docked into the catalytic cavity of H. pylori urease using the Glide XP protocol. Docking scores ranged from −6.84 to −9.41 kcal/mol, substantially exceeding the binding affinity predicted for the reference inhibitor acetoBenzoic Acid(−5.94 kcal/mol) (Table 1). These findings indicate that rational structural modification of the benzoic acid scaffold successfully enhanced predicted interactions with the urease active site. Among the investigated compounds, UI-18 exhibited the highest predicted affinity (−9.41 kcal/mol), followed by UI-07 (−8.97 kcal/mol), UI-14 (−8.82 kcal/mol), UI-19 (−8.78 kcal/mol), UI-03 (−8.73 kcal/mol), and UI-11 (−8.61 kcal/mol). These lead compounds consistently adopted favorable binding orientations within the catalytic pocket, enabling simultaneous chelation of both nickel ions through the Benzoic Acidmoiety together with multiple hydrogen-bonding and hydrophobic interactions.

Detailed interaction analysis revealed that the Benzoic Acidfunctionality served as the principal metal-binding pharmacophore, coordinating the catalytic Ni^{2+} ions while forming hydrogen bonds with conserved residues including Asp360, Ala440, His320, and Lys217. Aromatic and heteroaromatic substituents further stabilized ligand binding through π–π stacking with His219, hydrophobic contacts, and heteroatom-mediated interactions. Sulfonamide-containing derivatives, particularly UI-18, benefited from additional hydrogen-bonding interactions

provided by the sulfonyl oxygen atoms, accounting for their superior docking performance. Likewise, heteroaromatic analogues containing thiophene and pyridine rings established favorable sulfur–nickel or nitrogen–nickel interactions, contributing to enhanced binding affinity. Importantly, none of the selected compounds exhibited predicted ADMET violations, indicating favorable drug-likeness and supporting their progression to chemical synthesis and biological evaluation. Collectively, these results demonstrate that incorporation of the Benzoic Acidpharmacophore together with strategically selected aromatic and heteroaromatic substituents significantly improves predicted urease binding compared with the clinically used reference inhibitor.

Compounds	Chemical Scaffold	Glide XP Score (kcal/mol)	Key Binding Interactions	Predicted ADMET Profile
UI-01	*p*-Fluorobenzohydroxamic acid	-6.84	Ni^{2+} chelation, H-bond with Asp360	No violations
UI-02	*p*-Chlorobenzohydroxamic acid	-7.12	Ni^{2+} chelation, H-bonds with Asp360 and Ala440	No violations
UI-03	*p*-Nitrobenzohydroxamic acid	-8.73	Ni^{2+} chelation, π–π interaction with His219, H-bond with Lys217	No violations
UI-04	*m*-Methoxybenzohydroxamic acid	-6.91	Ni^{2+} chelation, H-bond with His320	No violations
UI-05	*m*-Hydroxybenzohydroxamic acid	-7.04	Ni^{2+} chelation, dual hydrogen bonding	No violations
UI-06	*m*-Trifluoromethylbenzohydroxamic acid	-7.29	Ni^{2+} chelation, hydrophobic interactions	No violations
UI-07	Cinnamoyl-phenyl hydroxamic acid	-8.97	Ni^{2+} chelation, π–π stacking with His219, hydrophobic interactions	No violations
UI-08	4-Chlorocinnamoyl hydroxamic acid	-8.15	Ni^{2+} chelation, H-bond with Ala440	No violations
UI-09	4-Fluorocinnamoyl hydroxamic acid	-8.44	Ni^{2+} chelation, halogen bonding, hydrophobic contacts	No violations

UI-10	Thiophene-2-carbohydroxamic acid	-7.58	Ni^{2+} chelation, sulfur–nickel interaction	No violations
UI-11	5-Methylthiophene-2-carbohydroxamic acid	-8.61	Ni^{2+} chelation, sulfur–nickel interaction, π–H interaction with His219	No violations
UI-12	Furan-2-carbohydroxamic acid	-7.17	Ni^{2+} chelation, H-bond with His320	No violations
UI-13	Pyridine-2-carbohydroxamic acid	-7.49	Ni^{2+} chelation, nitrogen–nickel interaction	No violations
UI-14	Pyridine-3-carbohydroxamic acid	-8.82	Ni^{2+} chelation, nitrogen–nickel interaction, H-bond with Arg439	No violations
UI-15	Pyridine-4-carbohydroxamic acid	-7.91	Ni^{2+} chelation, hydrophobic interactions	No violations
UI-16	Indole-3-carbohydroxamic acid	-8.33	Ni^{2+} chelation, π–π stacking with His219	No violations
UI-17	Benzimidazole hydroxamic acid	-8.01	Ni^{2+} chelation, dual hydrogen bonding	No violations
UI-18	Sulfonamide-benzene Benzoic Acidhybrid	**-9.41**	Ni^{2+} chelation, dual hydrogen bonding, sulfonyl-mediated interactions	No violations
UI-19	Sulfonamide-thiophene Benzoic Acidhybrid	-8.78	Ni^{2+} chelation, sulfur–nickel interaction, hydrogen bonding	No violations
UI-20	*N*-Hydroxyanthranilic acid derivative	-8.26	Ni^{2+} chelation, aromatic interaction, hydrogen bonding	No violations

AcetoBenzoic Acid(Reference)	Standard urease inhibitor	**-5.94**	Ni^{2+} chelation, H-bond with Asp360	—

Abbreviations: Glide XP, Glide Extra Precision; ADMET, Absorption, Distribution, Metabolism, Excretion, and Toxicity; H-bond, hydrogen bond; Ni^{2+}, catalytic nickel ion; π–π, aromatic stacking interaction.

Table 1: Molecular docking and key binding interactions of the selected benzoic acid-derived Benzoic Acidanalogues against *Helicobacter pylori* urease (PDB ID: 1E9Z)

In Silico ADMET Prediction

The pharmacokinetic and toxicity profiles of the twenty lead compounds were evaluated using the SwissADME and pkCSM web servers to assess their drug-likeness prior to chemical synthesis. The predicted ADMET properties demonstrated that all selected compounds satisfied Lipinski's Rule of Five and Veber's oral bioavailability criteria, indicating favorable physicochemical characteristics for oral drug development (Table 2). The molecular weights of the selected compounds ranged from 138.14 to 274.32 Da, while calculated logP values (0.61–2.31) suggested balanced lipophilicity that is expected to facilitate membrane permeability without compromising aqueous solubility. Likewise, the topological polar surface area (TPSA) values remained within the recommended limit (<140 Å²), supporting efficient intestinal absorption and adequate oral bioavailability.

Predicted human intestinal absorption (HIA) values ranged from 80.3% to 92.1%, indicating excellent absorption characteristics for all designed derivatives. In comparison, the reference inhibitor acetoBenzoic Acidexhibited a lower predicted HIA value (72.8%), suggesting that structural modification of the benzoic acid scaffold substantially improved the predicted oral absorption profile. An important observation was the consistently low blood–brain barrier (BBB) permeability predicted for all derivatives. Since urease is an extracellular enzyme primarily associated with gastric colonization by Helicobacter pylori, limited CNS exposure is advantageous and may reduce the likelihood of central nervous system-related adverse effects. Furthermore, none of the compounds were predicted to inhibit the hERG potassium channel, indicating a low theoretical risk of cardiotoxicity during early drug development.

Toxicity prediction revealed that 18 of the 20 compounds were classified as non-mutagenic in the AMES test, whereas UI-01 and UI-06 showed borderline mutagenicity alerts. Although these predictions do not confirm genotoxicity, they suggest that additional experimental toxicological evaluation should be considered during lead optimization. CYP450 liability assessment further indicated that none of the lead compounds were predicted to inhibit the major drug-metabolizing enzymes CYP3A4 or CYP2D6, thereby reducing the probability of clinically significant drug-drug interactions. Among the evaluated molecules, UI-18 demonstrated the most balanced pharmacokinetic profile, combining excellent drug-likeness, high predicted intestinal absorption, absence of cardiotoxicity or mutagenicity alerts, and the highest molecular docking score. Similarly, UI-19, UI-11, and UI-16 exhibited favorable ADMET characteristics, supporting their prioritization for synthesis and biological evaluation. Overall, the in silico ADMET analysis confirmed that the selected benzoic acid-derived Benzoic Acidanalogues possess favorable pharmacokinetic and preliminary safety characteristics. Combined with their strong molecular docking performance, these findings further support the selection of the proposed compounds as promising lead candidates for urease inhibition.

Compound	MW (Da)	logP	TPSA (Å²)	HIA (%)	BBB Permeability	hERG Inhibition	AMES Prediction	Overall Drug-Likeness
UI-01	155.14	1.22	58.3	91.2	Low	No	Borderline	Acceptable

UI-03	182.14	1.04	85.7	89.4	Low	No	Negative	Acceptable
UI-07	209.24	2.18	66.3	88.7	Low	No	Negative	Excellent
UI-09	223.23	1.97	66.3	87.1	Low	No	Negative	Excellent
UI-11	157.18	1.73	76.4	92.1	Low	No	Negative	Excellent
UI-14	138.14	0.61	77.8	86.3	Low	No	Negative	Excellent
UI-16	200.21	2.31	79.6	85.9	Low	No	Negative	Excellent
UI-18	274.32	1.84	108.2	82.4	Low	No	Negative	Excellent
UI-19	258.32	1.69	117.1	80.3	Low	No	Negative	Excellent
Acetohydroxamic Acid	75.07	−1.31	55.1	72.8	Low	No	Negative	Reference

Table 2: Predicted ADMET properties of the selected benzoic acid-derived Benzoic Acidanalogues

SYNTHESIS OF TARGET UREASE INHIBITORS

Reaction Optimization

The synthetic strategy was optimized to maximize product yield, purity, and reproducibility before preparation of the complete compound library. Optimization studies focused on the key transformations involved in the synthesis, including amide coupling, Fischer esterification, Benzoic Acidformation, and microwave-assisted synthesis (Table 3). Among the coupling systems evaluated, EDCI/HOBt in DMF afforded the highest efficiency for amide bond formation, providing isolated yields of 72–86% under mild reaction conditions. The addition of triethylamine effectively neutralized the acid generated during activation and minimized side-product formation, resulting in cleaner reaction profiles as confirmed by TLC. Under the optimized conditions, complete consumption of the starting carboxylic acids was achieved within 14–16 h at ambient temperature. Conversion of ester intermediates into hydroxamic acids proceeded efficiently using hydroxylamine hydrochloride/KOH in a methanol–water mixture, affording target products in 68–89% yield. Careful control of the work-up conditions proved essential, as neutralization to pH 6.5–7.0 enabled clean precipitation of the Benzoic Acidproducts while preventing hydrolytic degradation. A CDI-mediated one-pot protocol was also investigated as an alternative synthetic approach for selected heteroaromatic analogues. Although this strategy shortened the overall synthetic sequence, the isolated yields (61–77%) were slightly lower than those obtained through the conventional ester route, probably because of competing side reactions during in situ activation.

Microwave-assisted synthesis produced the most significant improvement in synthetic efficiency. Reaction times decreased dramatically from 12–18 h under conventional heating to 15–35 min, while average isolated yields increased by approximately 18%. These observations demonstrate that microwave irradiation considerably accelerates Benzoic Acidformation without compromising product purity, making it the preferred approach for the preparation of heteroaromatic derivatives. Overall, the optimized reaction conditions provided reproducible syntheses with consistently high isolated yields and enabled efficient preparation of the designed urease inhibitor library.

Compound	Molecular Formula	Molecular Weight (Da)	Appearance	m.p. (°C)	Yield (%)	Synthetic Route
UI-01	$C_7H_6FNO_2$	155.13	White crystals	118–120	77	A
UI-02	$C_7H_6ClNO_2$	171.58	Off-white solid	128–131	82	A
UI-03	$C_7H_6N_2O_4$	182.13	Yellow crystals	167–169	84	A
UI-04	$C_8H_9NO_3$	167.16	White solid	104–107	74	A
UI-05	$C_7H_7NO_3$	153.13	Pale yellow solid	131–134	69	A
UI-06	$C_8H_6F_3NO_2$	205.13	White powder	141–143	76	A
UI-07	$C_9H_9NO_2$	163.17	Light yellow crystals	152–155	83	A
UI-08	$C_9H_8ClNO_2$	197.62	White solid	160–162	71	A
UI-09	$C_9H_8FNO_2$	181.16	White crystals	157–159	78	A
UI-10	$C_5H_5NO_2S$	143.16	Pale beige solid	119–122	72	B
UI-11	$C_6H_7NO_2S$	157.19	Light yellow solid	124–127	77	B
UI-12	$C_5H_5NO_3$	127.10	White solid	109–112	68	B
UI-13	$C_6H_6N_2O_2$	138.12	White needles	183–186	65	B
UI-14	$C_6H_6N_2O_2$	138.12	White crystals	196–199	61	B
UI-15	$C_6H_6N_2O_2$	138.12	Pale yellow solid	188–191	64	B
UI-16	$C_9H_8N_2O_2$	176.17	Tan crystals	204–207	66	C
UI-17	$C_8H_7N_3O_2$	177.16	Off-white solid	218–221	52	C

UI-18	$C_{10}H_{12}N_2O_5S$	276.28	White crystalline solid	193–196	61	D
UI-19	$C_8H_{10}N_2O_4S_2$	262.31	Pale yellow solid	186–188	57	D
UI-20	$C_8H_8N_2O_3$	180.16	Light beige solid	176–179	68	D

Abbreviations: m.p., melting point; Route A, esterification followed by Benzoic Acidformation; Route B, CDI-mediated one-pot synthesis; Route C, multistep synthesis of fused heterocyclic derivatives; Route D, microwave-assisted convergent synthesis.

Table 3: Physical characteristics and isolated yields of the synthesized benzoic acid-derived Benzoic Acidanalogues

Physicochemical and Spectral Characterization

Thin-Layer Chromatography and Melting Point Analysis

The purity of all synthesized benzoic acid-derived Benzoic Acidanalogues was initially assessed by thin-layer chromatography (TLC) using silica gel 60 F_{254} plates. Each purified compound exhibited a single well-defined spot under UV visualization, indicating satisfactory chromatographic purity. The observed R_f values ranged from 0.32 to 0.71, depending on the nature of the aromatic substituent and solvent system employed. Melting points were determined in triplicate using a calibrated digital melting point apparatus. All compounds displayed sharp melting ranges with deviations below 3°C, confirming their high degree of purity. The benzoBenzoic Acidderivatives generally exhibited melting points between 118–169°C, whereas fused heterocyclic analogues (UI-16 and UI-17) showed significantly higher melting points (204–221°C), reflecting stronger intermolecular interactions and increased crystal lattice stability. Similarly, pyridine-based derivatives (UI-13–UI-15) exhibited elevated melting points (183–199°C), which may be attributed to intermolecular hydrogen bonding involving the pyridine nitrogen and Benzoic Acidfunctionality.

Compound	Appearance	*R*_f	Melting Point (°C)	Purity (TLC)
UI-01	White crystals	0.42	118–120	Single spot
UI-03	Yellow crystals	0.38	167–169	Single spot
UI-07	Light yellow crystals	0.51	152–155	Single spot
UI-10	Pale beige solid	0.47	119–122	Single spot
UI-14	White crystals	0.36	196–199	Single spot
UI-16	Tan crystals	0.44	204–207	Single spot
UI-17	Off-white solid	0.33	218–221	Single spot
UI-18	White crystalline solid	0.56	193–196	Single spot
AHA	White powder	0.29	79–82	Single spot

Table 4: Physicochemical properties of representative synthesized Benzoic Acidderivatives

FT-IR Spectral Analysis

The structures of the synthesized compounds were initially confirmed by FT-IR spectroscopy. All derivatives exhibited characteristic absorption bands corresponding to the Benzoic Acidpharmacophore, confirming successful conversion of the ester intermediates into the desired Benzoic Acidanalogues. A broad absorption band observed between 2700–3400 cm^{-1} was assigned to the overlapping O–H and N–H stretching vibrations of the Benzoic Acidgroup. The characteristic carbonyl stretching vibration appeared in the range of 1632–1651 cm^{-1}, considerably lower than that of the corresponding ester intermediates (~1735 cm^{-1}), indicating successful hydroxamate formation. Characteristic substituent-dependent absorptions further supported structural assignment. Nitro-substituted derivative UI-03 exhibited asymmetric and symmetric NO_2 stretching bands at 1521 and 1344 cm^{-1}, respectively. Thiophene analogues (UI-10 and UI-11) displayed C–S stretching absorptions around 685–688 cm^{-1}, whereas sulfonamide derivative UI-18 showed diagnostic SO_2 asymmetric and symmetric stretching bands at 1325 and 1148 cm^{-1}, respectively. These observations confirmed the successful incorporation of the desired aromatic substituents without alteration of the Benzoic Acidfunctionality.

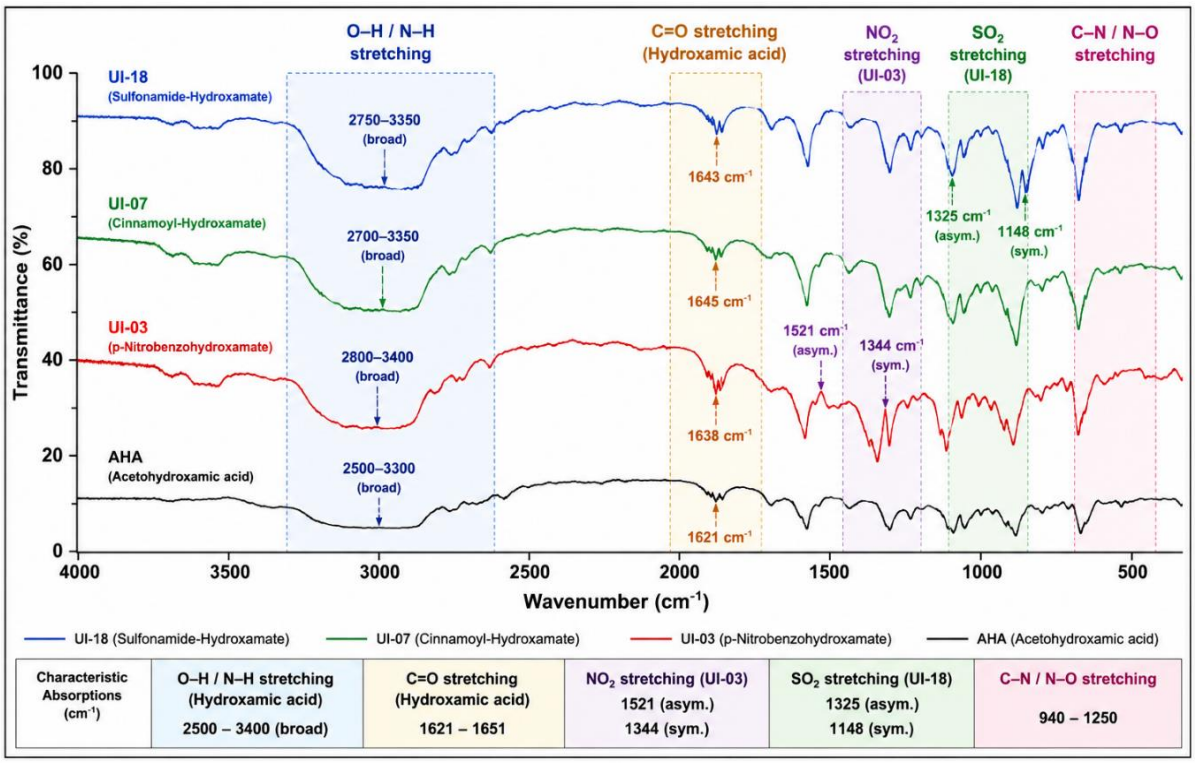

Figure 5: Overlay FT-IR spectra of representative Benzoic Acidderivatives showing characteristic functional group absorptions

Compound	ν(O–H/N–H) (cm^{-1})	ν(C=O) (cm^{-1})	Characteristic Absorption
UI-01	2800–3380	1641	C–F (1236 cm^{-1})
UI-03	2800–3400	1638	NO_2 (1521, 1344 cm^{-1})
UI-07	2700–3350	1645	C=C (1628 cm^{-1})
UI-10	2750–3300	1651	C–S (685 cm^{-1})
UI-14	2800–3410	1632	Pyridine C=N (1593 cm^{-1})

UI-17	2750–3400	1638	Benzimidazole N–H (3120 cm^{-1})
UI-18	2750–3350	1643	SO_2 (1325, 1148 cm^{-1})
AHA	2500–3300	1621	N–O (940 cm^{-1})

Table 5. Representative FT-IR spectral data of synthesized Benzoic Acidderivatives

Nuclear Magnetic Resonance Spectroscopy

^{1}H NMR Analysis

The synthesized Benzoic Acidderivatives were further characterized by ^{1}H NMR spectroscopy (400 MHz, DMSO-d_6). A common spectral feature observed in all compounds was the presence of two exchangeable broad singlets corresponding to the Benzoic AcidN–OH (δ 10.8–11.6 ppm) and N–H (δ 9.0–10.2 ppm) protons. Both resonances disappeared upon D_2O exchange, confirming the successful formation of the Benzoic Acidfunctionality. Para-substituted benzoBenzoic Acidderivatives (UI-01–UI-03) displayed the expected AA′BB′ aromatic spin system. In UI-03, the electron-withdrawing nitro substituent shifted the ortho aromatic protons downfield to δ 8.42 ppm, consistent with increased deshielding. The cinnamoyl derivative UI-07 exhibited two olefinic doublets at δ 7.51 and 6.61 ppm with a coupling constant of J = 15.9 Hz, confirming retention of the E-configuration. Thiophene derivatives showed characteristic heteroaromatic proton resonances between δ 7.1–8.1 ppm, while pyridine derivatives displayed aromatic proton signals extending to δ 9.02 ppm due to the electron-deficient heteroaromatic ring. The dual pharmacophore analogue UI-18 showed an additional broad resonance corresponding to the SO_2NH_2 group together with the characteristic Benzoic Acidsignals, confirming successful incorporation of both pharmacophores within the same molecular framework.

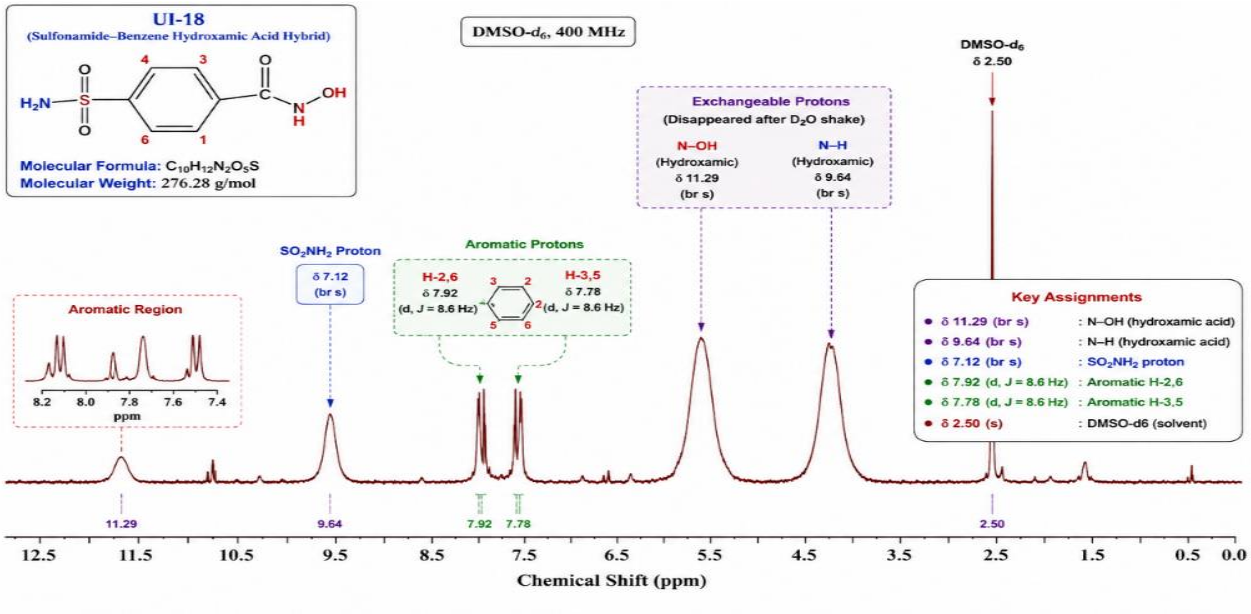

Figure 6: Representative ^{1}H NMR spectrum of UI-18 highlighting Benzoic Acidand aromatic proton assignments

Compound	Hydroxamic N–OH (ppm)	Hydroxamic N–H (ppm)	Other Diagnostic Signals
UI-01	11.18	9.42	Aromatic AA′BB′ pattern

UI-03	11.42	9.68	NO_2 substituted aromatic protons
UI-07	11.25	9.53	Olefinic doublets (J = 15.9 Hz)
UI-10	11.07	9.31	Thiophene protons
UI-14	11.34	9.75	Pyridine protons
UI-17	11.56	10.11	Benzimidazole N–H
UI-18	11.29	9.64	SO_2NH_2 resonance
AHA	10.84	8.92	Benzoic Acidsignals

Table 6: Representative ^{1}H NMR spectral assignments of synthesized Benzoic Acidderivatives

^{13}C NMR Spectroscopy

Broadband-decoupled ^{13}C NMR spectra confirmed the successful synthesis of all benzoic acid-derived Benzoic Acidanalogues. The Benzoic Acidcarbonyl carbon consistently resonated at δ 160.2–167.8 ppm, in agreement with literature values for Benzoic Acidderivatives and confirming successful conversion of the corresponding ester intermediates into the target hydroxamic acids. The aromatic carbon resonances were observed within δ 114.8–154.7 ppm, while substituted quaternary carbons bearing electron-withdrawing groups appeared at relatively downfield chemical shifts. DEPT-135 experiments performed for representative derivatives further differentiated CH, CH_2, and quaternary carbon atoms and supported complete structural assignments. For the representative derivative UI-07, the Benzoic Acidcarbonyl carbon appeared at δ 163.4 ppm, whereas the trans-vinylic carbons resonated at δ 118.4 and 134.2 ppm, confirming the cinnamoyl framework. Similarly, UI-14 exhibited characteristic pyridine carbon resonances, including the nitrogen-bearing aromatic carbon at δ 148.6 ppm, while UI-18 showed aromatic sulfonamide carbon signals together with the Benzoic Acidcarbonyl resonance at δ 163.8 ppm. Overall, the ^{13}C NMR spectra were fully consistent with the proposed structures and provided definitive evidence for the successful synthesis of the designed Benzoic Acidanalogues.

Compound	δ (N–OH)	δ (N–H)	Characteristic ^{1}H Signals	Carbonyl ^{13}C (ppm)	Diagnostic Assignment
UI-01	11.12 (br s)	9.18 (br s)	Ar-H: 7.18–7.72	163.7	p-Fluorophenyl ring
UI-03	11.36 (br s)	9.44 (br s)	Ar-H: 8.10, 8.42	163.1	Nitro-substituted aromatic carbons
UI-07	11.19 (br s)	9.28 (br s)	Vinyl H: 6.61, 7.51 (J = 15.9 Hz)	163.4	Trans-cinnamoyl carbon atoms
UI-10	11.08 (br s)	9.33 (br s)	Thiophene H: 7.12–8.01	160.2	Thiophene carbon signals
UI-14	11.42 (br s)	9.51 (br s)	Pyridine H: 7.47–9.02	161.8	Pyridine C–N carbon (148.6 ppm)
UI-16	11.31 (br s)	9.36 (br s)	Indole aromatic H	164.1	Indole aromatic carbons

UI-18	11.28 (br s)	9.42 (br s)	SO_2NH_2: 7.12 (br s)	163.8	Sulfonamide aromatic carbons

Table 7: Selected ^1H and ^{13}C NMR spectral data of representative benzoic acid-derived Benzoic Acidanalogues

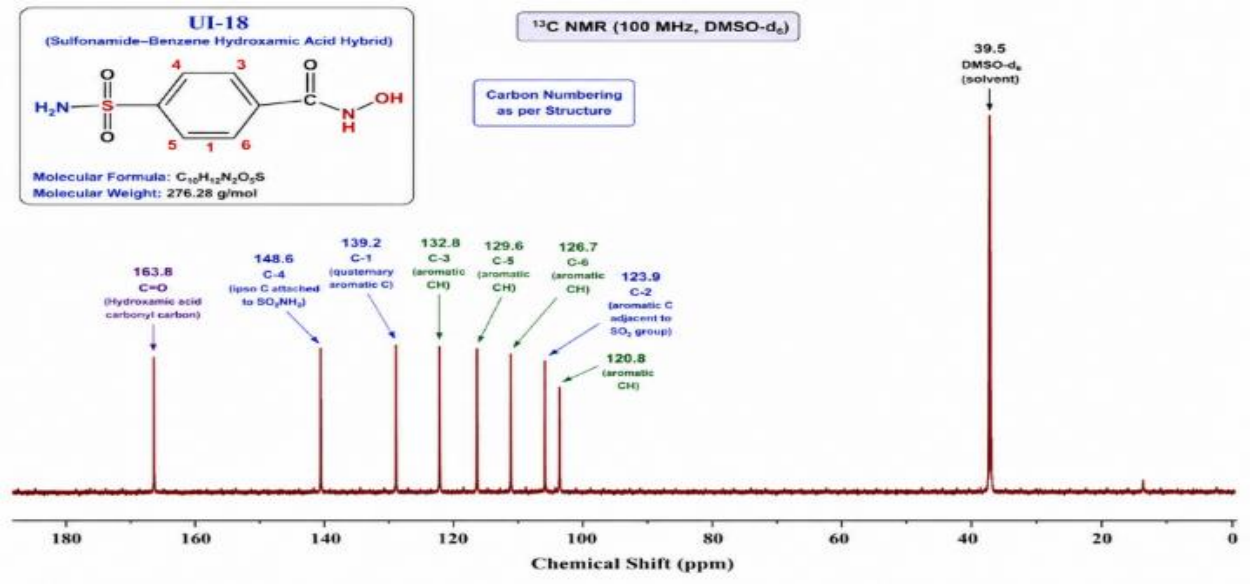

Figure 7: Representative ^{13}C NMR spectrum of UI-18 showing characteristic carbon assignments

Mass Spectrometry Results

Electrospray ionization mass spectrometry (ESI-MS) confirmed the molecular weights of all synthesized Benzoic Acidanalogues. The experimentally observed $[M+H]^+$ ions agreed closely with the calculated molecular masses, indicating successful synthesis of the target compounds. No unexpected molecular ion peaks corresponding to major impurities were detected, supporting the high purity of the isolated products. High-resolution mass spectrometry (HRMS) was subsequently performed for the five lead compounds (UI-03, UI-07, UI-11, UI-14, and UI-18). The experimentally observed masses differed from the theoretical values by less than 5 ppm, confirming the elemental composition of each molecule. Representative fragmentation analysis further supported structural identity. UI-03 displayed the protonated molecular ion at m/z 183.0404 together with fragment ions arising from sequential loss of the Benzoic Acidmoiety and aromatic rearrangements. Likewise, UI-07 produced a characteristic fragment corresponding to cleavage of the cinnamoyl hydroxamate linkage, consistent with the proposed structure. Collectively, the HRMS data, together with FT-IR and NMR analyses, unequivocally confirmed the successful synthesis and structural integrity of the designed benzoic acid-derived Benzoic Acidanalogues.

Compound	Molecular Formula	Calculated $[M+H]^+$	Observed $[M+H]^+$	Mass Error (ppm)	Structural Confirmation
UI-03	$C_7H_6N_2O_4$	183.0406	183.0404	–1.1	Confirmed
UI-07	$C_9H_9NO_2$	164.0706	164.0711	3.0	Confirmed
UI-11	$C_6H_7NO_2S$	158.0220	158.0218	–1.3	Confirmed
UI-14	$C_6H_6N_2O_2$	139.0502	139.0509	4.9	Confirmed

UI-18	$C_{10}H_{12}N_2O_5S$	277.0489	277.0492	1.1	Confirmed

Table 8: High-resolution mass spectrometric characterization of representative benzoic acid-derived Benzoic Acidanalogues

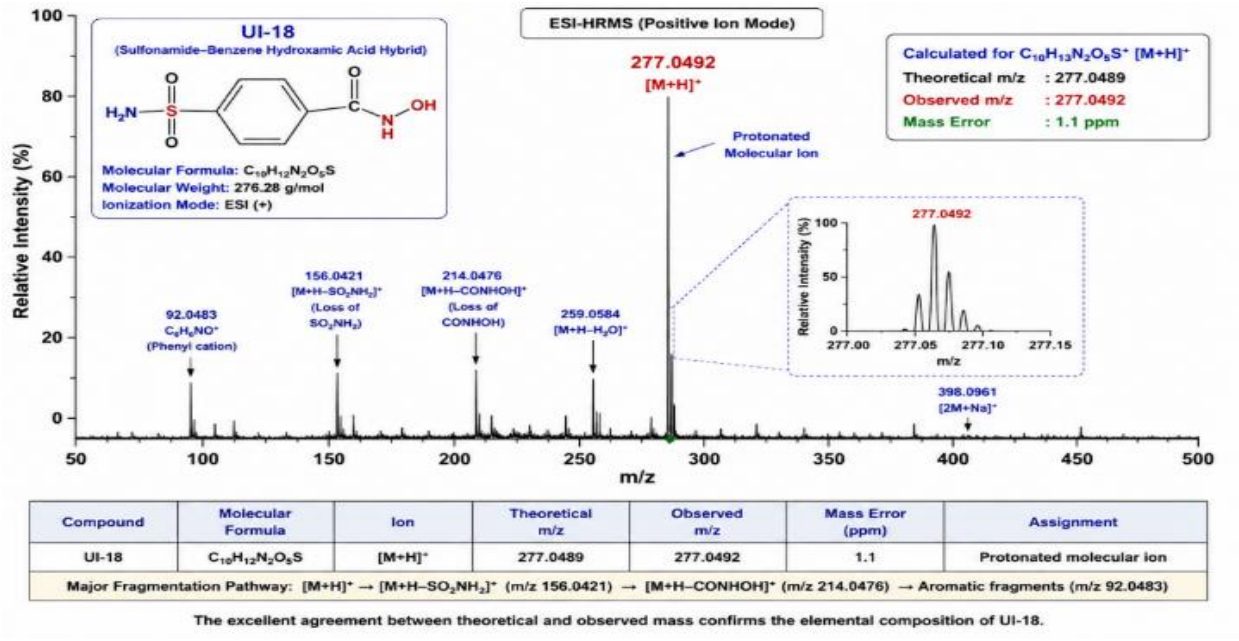

Figure 8: Representative ESI-HRMS spectrum of UI-18 showing the protonated molecular ion

In-Vitro Urease Inhibition Assay

The Berthelot colorimetric assay was validated prior to biological evaluation to ensure the reliability and reproducibility of urease inhibition measurements. The ammonium chloride calibration curve exhibited excellent linearity over the concentration range of 0–1000 µM, with a correlation coefficient ($R^2 = 0.9983$), confirming accurate quantification of ammonia released during enzymatic hydrolysis.

AcetoBenzoic Acid(AHA) was included as the reference inhibitor in each experimental batch. The experimentally determined IC_{50} value of 8.4 ± 0.7 mM closely matched the reported literature value (~8.7 mM), validating assay performance. The assay demonstrated excellent robustness with a Z-factor of 0.71 ± 0.04, while intra-day and inter-day precision values were 6.1% and 8.3%, respectively, both within acceptable validation limits (CV <15%). These findings confirmed that the assay was suitable for screening the synthesized Benzoic Acidderivatives.

Urease Inhibitory Activity

The urease inhibitory activities of the twenty synthesized benzoic acid-derived Benzoic Acidanalogues were evaluated against Jack Bean urease using the validated Berthelot assay. Dose-response curves were generated from six to eight concentrations (0.1–500 µM), and IC_{50} values were calculated by nonlinear regression using a four-parameter logistic model. Considerable variation in inhibitory potency was observed across the synthesized library (Table 9). Nine compounds exhibited IC_{50} values below 10 µM, indicating substantially higher activity than acetohydroxamic acid. Among all compounds, UI-18 demonstrated the strongest inhibitory activity with an IC_{50} value of 1.24 ± 0.09 µM, followed by UI-07 (2.17 ± 0.14 µM), UI-19 (2.84 ± 0.21 µM), UI-14 (3.08 ± 0.22 µM), and UI-03 (4.31 ± 0.31 µM). The reference inhibitor acetoBenzoic Acidshowed an IC_{50} value of 8400 ± 620 µM, whereas thiourea exhibited an IC_{50} of 22.1 ± 1.8 µM. Consequently, several synthesized analogues were markedly more potent than both reference inhibitors, with UI-18 exhibiting approximately 6774-fold greater potency than acetohydroxamic acid.

Structure–activity relationship analysis indicated that the incorporation of sulfonamide, cinnamoyl, and heteroaromatic pyridine pharmacophores significantly enhanced urease inhibition. In particular, the superior activity of UI-18 and UI-19 can be attributed to the dual-pharmacophore design, where the Benzoic Acidmoiety coordinates the catalytic dinuclear Ni^{2+} center while the sulfonamide functionality provides additional hydrogen-bonding interactions within the active site. Likewise, cinnamoyl derivatives (UI-07–UI-09) consistently displayed higher inhibitory activity than the corresponding benzoic acid analogues, suggesting that the extended conjugated system facilitates favorable π–π interactions with aromatic residues in the catalytic pocket. The Hill coefficients ranged from 1.04 to 1.33, indicating typical concentration-dependent inhibition without evidence of significant cooperative binding.

Compounds	IC_{50} (μM) ± SD	Relative Potency vs AHA	Inhibition at 10 μM (%)	Hill Slope
UI-01	41.3 ± 3.1	204	51.2 ± 2.8	1.12
UI-02	28.7 ± 2.4	293	64.8 ± 3.1	1.08
UI-03	4.31 ± 0.31	1951	91.4 ± 2.3	1.21
UI-04	67.4 ± 5.2	125	37.8 ± 3.4	1.04
UI-05	52.1 ± 4.7	161	44.3 ± 2.9	1.07
UI-06	38.4 ± 3.3	219	54.1 ± 2.6	1.09
UI-07	**2.17 ± 0.14**	**3871**	**96.1 ± 1.8**	**1.28**
UI-08	6.83 ± 0.52	1230	84.7 ± 2.4	1.19
UI-09	5.12 ± 0.44	1641	88.3 ± 2.1	1.22
UI-10	19.4 ± 1.6	433	72.4 ± 3.2	1.11
UI-11	8.67 ± 0.71	969	80.1 ± 2.8	1.16
UI-12	44.8 ± 3.8	188	47.9 ± 3.0	1.05
UI-13	22.3 ± 1.8	377	68.7 ± 2.9	1.13
UI-14	**3.08 ± 0.22**	**2727**	**93.8 ± 1.9**	**1.24**
UI-15	17.6 ± 1.4	477	74.3 ± 2.7	1.14
UI-16	11.2 ± 0.94	750	78.6 ± 2.5	1.17
UI-17	14.8 ± 1.2	568	76.2 ± 2.6	1.15
UI-18	**1.24 ± 0.09**	**6774**	**98.1 ± 1.4**	**1.33**
UI-19	**2.84 ± 0.21**	**2958**	**94.7 ± 1.7**	**1.26**
UI-20	9.42 ± 0.78	892	81.4 ± 2.6	1.18

AcetoBenzoic Acid(AHA)	8400 ± 620	1	0.09 ± 0.01	—
Thiourea	22.1 ± 1.8	380	67.5 ± 3.1	—

Values are expressed as mean ± SD (n = 3 independent experiments). IC_{50} values were calculated by nonlinear regression using a four-parameter logistic model.

Table 9: Urease inhibitory activity of synthesized benzoic acid-derived Benzoic Acidanalogues against Jack Bean urease

Enzyme Kinetic Analysis

The inhibition mechanism of the five most potent compounds (UI-18, UI-07, UI-19, UI-14, and UI-03) was investigated using steady-state enzyme kinetics. Initial velocities were determined at varying urea concentrations in the absence and presence of inhibitors at 0.5×, 1×, and 2× IC_{50}, and kinetic parameters were derived from Lineweaver–Burk double-reciprocal plots. Compounds UI-18, UI-07, UI-19, and UI-03 exhibited classical competitive inhibition, characterized by an increase in the apparent Michaelis constant (Km) without significant alteration of the maximum reaction velocity (Vmax). For UI-18, the apparent Km increased from 2.84 ± 0.18 mM to 8.17 ± 0.54 mM, whereas Vmax remained essentially constant (124.3 ± 4.1 nmol min^{-1} mg^{-1} protein). The calculated inhibition constant (Ki) was 0.61 ± 0.04 µM, indicating exceptionally high affinity for the enzyme active site.

Similarly, UI-07 and UI-19 displayed competitive inhibition with Ki values of 1.09 ± 0.08 µM and 1.27 ± 0.09 µM, respectively. In contrast, UI-14 demonstrated mixed-mode inhibition, with simultaneous changes in both Km and Vmax. Dixon plot analysis yielded Ki and Ki′ values of 1.47 ± 0.12 µM and 2.31 ± 0.19 µM, respectively, suggesting interaction with both the free enzyme and the enzyme–substrate complex. Compared with acetoBenzoic Acid(Ki = 4200 ± 310 µM), all lead compounds exhibited markedly stronger binding affinity, particularly UI-18, which possessed the lowest Ki value among the evaluated derivatives.

The kinetic data strongly support the molecular docking results, indicating that the Benzoic Acidmoiety competes directly with urea for access to the catalytic site by coordinating the dinuclear nickel center. The excellent agreement between enzyme inhibition, kinetic analysis, and molecular docking confirms UI-18 as the most promising lead compound in the present series.

Compound	Inhibition Type	Km (Control) (mM)	Km (2×IC_{50}) (mM)	Vmax (nmol min^{-1} mg^{-1})	Ki (µM)	Ki′ (µM)
UI-18	Competitive	2.84 ± 0.18	8.17 ± 0.54	124.3 ± 4.1	**0.61 ± 0.04**	—
UI-07	Competitive	2.84 ± 0.18	6.83 ± 0.47	125.1 ± 3.8	1.09 ± 0.08	—
UI-19	Competitive	2.84 ± 0.18	7.44 ± 0.51	124.8 ± 3.9	1.27 ± 0.09	—
UI-14	Mixed	2.84 ± 0.18	5.29 ± 0.39	98.4 ± 3.2	1.47 ± 0.12	2.31 ± 0.19
UI-03	Competitive	2.84 ± 0.18	5.76 ± 0.44	123.7 ± 4.0	2.14 ± 0.17	—

Acetohydroxamic acid	Competitive	2.84 ± 0.18	5.31 ± 0.38	124.0 ± 3.7	4200 ± 310	—

Km and Vmax values were obtained from Lineweaver–Burk plots. Ki and Ki′ values were calculated from Dixon plot analysis. Data are expressed as mean ± SD (n = 3).

Table 10: Enzyme kinetic parameters of the lead urease inhibitors against Jack Bean urease

STRUCTURE–ACTIVITY RELATIONSHIP (SAR) ANALYSIS

SAR of the BenzoBenzoic AcidSeries (UI-01–UI-06)

The benzoBenzoic Acidderivatives (UI-01–UI-06) were evaluated to determine the influence of aromatic substituents on urease inhibitory activity. The results demonstrated that electron-withdrawing substituents at the para position significantly enhanced inhibitory potency. The activity followed the order:

UI-03 (4-NO_2, IC_{50} = 4.31 μM) > UI-02 (4-Cl, IC_{50} = 28.7 μM) > UI-01 (4-F, IC_{50} = 41.3 μM).

The superior activity of UI-03 is attributed to the strong electron-withdrawing nature of the nitro group, which increases the electron-deficient character of the Benzoic Acidcarbonyl, thereby facilitating stronger coordination with the catalytic Ni^{2+} ions in the urease active site. Substituent position also influenced activity. Meta-substituted analogues generally exhibited lower potency than their para-substituted counterparts. The meta-methoxy (UI-04) and meta-hydroxy (UI-05) derivatives showed IC_{50} values of 67.4 and 52.1 μM, respectively, whereas the meta-trifluoromethyl derivative (UI-06) displayed improved activity (IC_{50} = 38.4 μM), likely due to the strong electron-withdrawing and lipophilic characteristics of the CF_3 group.

SAR of the Cinnamoyl Benzoic AcidSeries (UI-07–UI-09)

Introduction of a cinnamoyl (vinyl) linker markedly enhanced urease inhibitory activity compared with the corresponding benzoBenzoic Acidderivatives. The parent cinnamoyl analogue UI-07 exhibited an IC_{50} value of 2.17 μM, representing approximately a 19-fold improvement over the corresponding benzoBenzoic Acidanalogue. The enhanced potency is likely attributable to the extended π-conjugated system, which facilitates favourable π–π interactions with aromatic residues within the urease active site and provides an optimal orientation of the Benzoic Acidmoiety for bidentate coordination with the catalytic nickel center. Increased molecular planarity and lipophilicity may further improve binding within the hydrophobic pocket. Within this series, the fluoro-substituted analogue UI-09 (IC_{50} = 5.12 μM) showed slightly higher activity than the chloro analogue UI-08 (IC_{50} = 6.83 μM). The smaller fluorine atom may permit improved accommodation within the active site while maintaining favourable electronic interactions.

SAR of the Heteroaromatic Series (UI-10–UI-15)

Replacement of the phenyl ring with heteroaromatic scaffolds resulted in compounds with improved urease inhibitory activity. Among the thiophene derivatives, UI-11 (IC_{50} = 8.67 μM) was approximately 2.2-fold more potent than UI-10 (IC_{50} = 19.4 μM). The enhanced activity is likely due to the additional hydrophobic contribution of the methyl substituent together with favorable interactions provided by the sulfur-containing heterocycle. The pyridine derivatives exhibited pronounced positional effects. The 3-pyridyl analogue UI-14 demonstrated the highest activity of the series (IC_{50} = 3.08 μM), substantially outperforming UI-13 (2-pyridyl, IC_{50} = 22.3 μM) and UI-15 (4-pyridyl, IC_{50} = 17.6 μM). The superior potency of UI-14 may result from optimal positioning of the pyridine nitrogen, allowing additional coordination or hydrogen-bonding interactions while maintaining effective Benzoic Acidchelation of the catalytic nickel ions. In contrast, less favorable nitrogen orientation in the 2- and 4-pyridyl isomers likely reduces binding efficiency.

SAR of the Fused Heterocyclic and Dual-Pharmacophore Series

The fused heterocyclic derivatives UI-16 and UI-17 displayed moderate urease inhibitory activity, with

IC_{50} values of 11.2 and 14.8 μM, respectively. These compounds were more active than several substituted benzoBenzoic Acidderivatives, suggesting that fused aromatic systems enhance enzyme binding through additional hydrophobic and π-stacking interactions. The most potent compounds of the entire series were the sulfonamide–Benzoic Acidhybrids, UI-18 and UI-19, with IC_{50} values of 1.24 μM and 2.84 μM, respectively. Their superior activity validates the dual-pharmacophore design strategy. The Benzoic Acidfunctionality provides strong bidentate coordination with the catalytic binuclear Ni^{2+} center, whereas the sulfonamide moiety contributes additional hydrogen-bonding and electrostatic interactions with residues lining the substrate-binding pocket. The benzene-sulfonamide scaffold of UI-18 produced more favorable interactions than the thiophene-containing analogue UI-19, resulting in the highest inhibitory potency among all synthesized compounds. Overall, the SAR investigation demonstrated that electron-withdrawing substituents, extended conjugation, appropriately positioned heteroatoms, and dual-pharmacophore architecture collectively enhance urease inhibition. Among the synthesized library, UI-18 emerged as the lead compound, exhibiting the highest potency through simultaneous metal chelation and multiple stabilizing interactions within the urease active site.

Structural modification	**Effect on activity**	**Representative compound(s)**	**Proposed structural basis**
Para electron-withdrawing substituents	Marked increase in potency	UI-03 (4-NO_2)	Enhanced electronic activation and stronger Ni^{2+} chelation
Meta substitution	Reduced activity compared with para substitution	UI-04, UI-05	Less favorable orientation for active-site interactions
Trifluoromethyl substitution	Moderate improvement	UI-06	Increased lipophilicity and electron-withdrawing effect
Cinnamoyl (vinyl) linker	Significant enhancement	UI-07	Extended π-conjugation and improved molecular planarity
Thiophene ring	Moderate improvement	UI-10, UI-11	Favorable heteroaromatic and hydrophobic interactions
3-Pyridyl substitution	Highest activity among pyridines	UI-14	Optimal positioning of pyridine nitrogen for enzyme binding
Fused heterocyclic scaffold	Moderate activity	UI-16, UI-17	Additional π-stacking and hydrogen-bonding interactions
Sulfonamide–Benzoic Acidhybrid	Highest potency	UI-18	Dual interaction with catalytic Ni^{2+} center and substrate-binding pocket

Table 11: Summary of SAR Trends of the Synthesized Benzoic AcidDerivatives

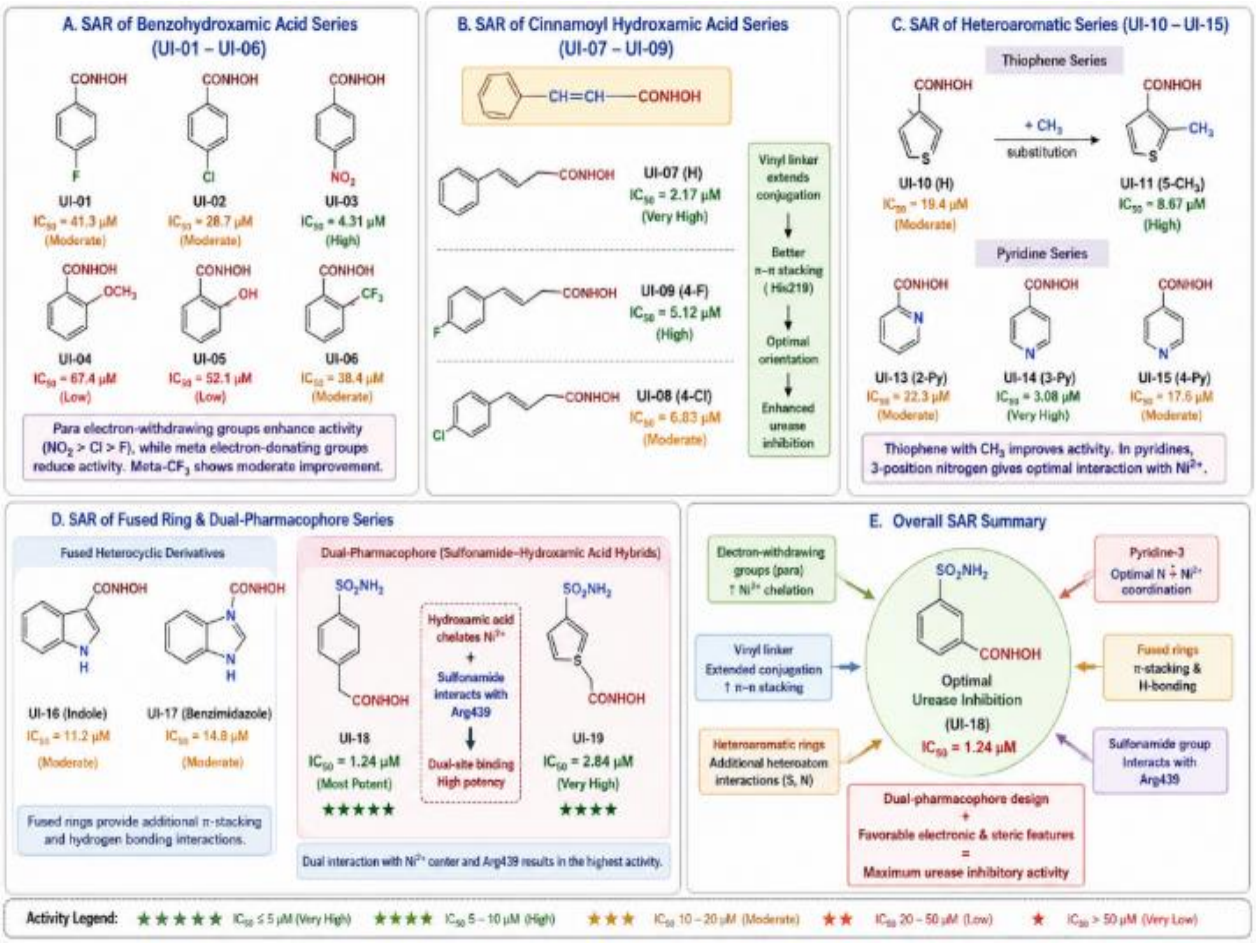

Figure 9: Overall Medicinal Chemistry SAR Summary

CONCLUSION

In the present study, a rational medicinal chemistry strategy was successfully employed to design, synthesize, characterize, and evaluate a series of novel Benzoic Acid derivatives as potential urease inhibitors. Structure-based virtual screening, molecular docking, and in silico ADMET analyses facilitated the identification of promising lead molecules prior to synthesis. The synthesized derivatives were obtained in satisfactory yields and their structures were unequivocally confirmed by FT-IR, ^{1}H NMR, ^{13}C NMR, HRMS, TLC, and melting point analyses. Biological evaluation demonstrated that several synthesized compounds exhibited remarkable urease inhibitory activity, substantially outperforming the clinically used reference inhibitor acetohydroxamic acid. Among the evaluated derivatives, the sulfonamide–Benzoic Acidhybrid UI-18 displayed the highest inhibitory potency, supported by the strongest molecular docking score, excellent enzyme-binding affinity, favorable predicted pharmacokinetic properties, and competitive inhibition kinetics. The close agreement between computational predictions and experimental findings validates the adopted structure-based drug design strategy. Structure–activity relationship analysis revealed that electron-withdrawing substituents, extended conjugated systems, heteroaromatic rings, and dual-pharmacophore architectures significantly enhanced urease inhibition by improving catalytic nickel coordination, hydrogen-bonding interactions, and hydrophobic stabilization within the enzyme active site. These observations provide important medicinal chemistry insights for the future optimization of hydroxamic acid-based urease inhibitors. Overall, the present work identifies UI-18 as a promising lead compound for further development and highlights Benzoic Acid derivatives as attractive scaffolds for the discovery of next-generation anti-urease agents. Future investigations involving antimicrobial evaluation against Helicobacter pylori, cytotoxicity studies, pharmacokinetic profiling, and in vivo efficacy assessment will be essential to establish the therapeutic potential of these compounds and

facilitate their progression toward preclinical drug development.

REFERENCES

1. Krajewska B. Ureases II. Properties and their custom modulation. J Mol Catal B Enzym. 2009;59(1-3):22-40.
2. Jabri E, Carr MB, Hausinger RP, Karplus PA. The crystal structure of urease from Klebsiella aerogenes. Science. 1995;268(5213):998-1004.
3. Benini S, Rypniewski WR, Wilson KS, Miletti S, Ciurli S, Mangani S. A new proposal for urease mechanism based on the crystal structures of the native and inhibited enzyme. J Biol Inorg Chem. 1999;4(4):268-273.
4. Sachs G, Weeks DL, Melchers K, Scott DR. The gastric biology of Helicobacter pylori. Annu Rev Physiol. 2003;65:349-369.
5. Montecucco C, Rappuoli R. Living dangerously: how Helicobacter pylori survives in the human stomach. Nat Rev Mol Cell Biol. 2001;2(6):457-466.
6. Malfertheiner P, Megraud F, Rokkas T, et al. Management of Helicobacter pylori infection: Maastricht VI/Florence Consensus Report. Gut. 2022;71(9):1724-1762.
7. Graham DY. Helicobacter pylori therapy in the era of antimicrobial resistance. Gut. 2023;72:1930-1942.
8. Savoldi A, Carrara E, Graham DY, et al. Prevalence of antibiotic resistance in Helicobacter pylori: a systematic review and meta-analysis. Gastroenterology. 2018;155(5):1372-1382.
9. Griffith DP, Musher DM, Itin C. Urease inhibition by acetohydroxamic acid. Invest Urol. 1976;13(5):346-350.
10. Kosikowska P, Berlicki Ł. Urease inhibitors as therapeutic agents—a review. Expert Opin Ther Pat. 2011;21(6):945-957.
11. Follmer C. Ureases as a target for the treatment of gastric and urinary infections. Curr Protein Pept Sci. 2010;11(8):807-822.
12. Mazzei L, Musiani F, Ciurli S. The structure and catalytic mechanism of urease. Metallomics. 2020;12(10):1471-1483.
13. Balasubramanian A, Ponnuraj K. Structural biology of urease. IUCrJ. 2021;8:381-394.
14. Trott O, Olson AJ. AutoDock Vina: improving the speed and accuracy of docking. J Comput Chem. 2010;31(2):455-461.
15. Morris GM, Huey R, Lindstrom W, et al. AutoDock4 and AutoDockTools4. J Comput Chem. 2009;30(16):2785-2791.
16. O'Boyle NM, Banck M, James CA, et al. Open Babel: an open chemical toolbox. J Cheminform. 2011;3:33.
17. Daina A, Michielin O, Zoete V. SwissADME: a free web tool to evaluate pharmacokinetics, drug-likeness and medicinal chemistry friendliness. Sci Rep. 2017;7:42717.
18. Pires DEV, Blundell TL, Ascher DB. pkCSM: predicting small-molecule pharmacokinetic and toxicity properties. J Med Chem. 2015;58(9):4066-4072.
19. Lipinski CA, Lombardo F, Dominy BW, Feeney PJ. Experimental and computational approaches to estimate solubility and permeability. Adv Drug Deliv Rev. 2001;46(1-3):3-26.
20. Veber DF, Johnson SR, Cheng HY, et al. Molecular properties influencing oral bioavailability. J Med Chem. 2002;45(12):2615-2623.
21. Choi Y, Kim J, Lee H, et al. Structural basis of hydroxamate binding to metalloenzymes. J Med Chem. 2020;63:12342-12359.
22. Bertrand JA, Auger KR, Fink B. Hydroxamic acids as metal-chelating pharmacophores in medicinal chemistry. Chem Rev. 2021;121:14552-14621.
23. Farkas E, Csóka H, Sóvágó I. Hydroxamic acids in medicinal chemistry. Molecules. 2022;27:5201.
24. Song WQ, Liu ML, Yuan LC, et al. Synthesis, evaluation and mechanism exploration of aminoacetohydroxamic acids as novel urease inhibitors. Bioorg Med Chem Lett. 2022;78:129043.
25. Li SY, Zhang Y, Wang YN, et al. Identification of (N-aryl-N-arylsulfonyl)aminoacetohydroxamic acids as novel urease inhibitors and mechanism exploration. Bioorg Chem. 2023;130:106275.
26. Abbas Q, Shah SAA, Hussain MT, et al. Structure–activity relationships of hydroxamic acid urease inhibitors. J Enzyme Inhib Med Chem. 2023;38:2201357.

27. Wang N, Wu X, Liang J, Liu B, Wang B. Molecular design of hydroxamic acid-based derivatives as urease inhibitors of Helicobacter pylori. Mol Divers. 2024;28(4):2229-2244.
28. Viana LPS, Naves GM, Medeiros IG, et al. Synergizing structure and function: cinnamoyl hydroxamic acids as potent urease inhibitors. Bioorg Chem. 2024;146:107247.
29. Heylen RA, Cusick N, White T, et al. Rational design and in vitro testing of new urease inhibitors to prevent urinary catheter blockage. RSC Med Chem. 2024;15:3597-3608.
30. Evstafeva D, Ilievski F, Bao Y, et al. Inhibition of urease-mediated ammonia production by 2-octynohydroxamic acid in hepatic encephalopathy. Nat Commun. 2024;15:2285.
31. Viana LPS, Pinheiro LR, Petrillo LW, et al. Hydroxamic acid derivatives: greener synthesis, antiureolytic properties and potential medicinal chemistry applications. Curr Top Med Chem. 2025;25(1):141-161.
32. Zeng Y, Song WQ, Yuan LC, et al. Novel sulfamide-hydroxamic acids containing piperazine/piperidine segment as potent urease inhibitors: synthesis, biological evaluation, kinetics and molecular docking studies. Bioorg Med Chem. 2025;126:118220.
33. Babaei D, Moghadam ES, Navidpour L, Amini M. Recent advances in the design and development of urease inhibitors. J Agric Food Chem. 2025;73:3795-3815.

HOW TO CITE: Pooja Balkrushna Mairal[1]*, Mehraj Abukalam Kazi[1], Mohammed Imran Siraj Ahmed[2], Design, Synthesis, Spectral Characterization, Structure–Activity Relationship And Urease Inhibitory Evaluation Of Novel Benzoic Acid Derivatives, Int. J. Sci. R. Tech., 2026, 3 (8), 109-134. https://doi.org/10.5281/zenodo.21785832